Fast Response Predictive Controllers for Mono-Inverter Dual Parallel Permanent Magnet Synchronous

M. Fadaie[a], K. Abbaszadeh[b*] , and A. Siadatan[c]

a. *Department of Electrical Engineering, Faculty of Electrical Engineering, Science and Research Branch, Islamic Azad University, Tehran, Iran (Tel: 05832228325, Mobile: 09153846314, Email: mehdi.fadaie.a@gmail.com).*
b. *Department of Electrical Engineering, Faculty of Electrical Engineering, K. N. Toosi University of Technology, Tehran, Iran (Tel: 02184062324, Mobile: 09122782695, Email:* abbaszadeh@kntu.ac.ir*).*
c. *Department of Electrical Engineering, College of Technical and Engineering West Tehran Branch, Islamic Azad University, Tehran, Iran (Mobile: 09121168606, Email: alireza.siadatan@iau.ac.ir).*

Abstract. The method of Mono-Inverter Dual-Parallel (MIDP) motors has been noticed in the drive of the multi-motor systems in order to reduce the number of power electronic devices as well as the volume, weight, and cost of the drive system. The load torque imbalance in motors has been one of the main problems of these systems because of feeding the motors by a single inverter. Some control methods have also been proposed in this field and studies are ongoing. This paper deals with an effective Model Predictive Control (MPC) method for the design of speed and current controllers in MIDP motors. Pontryagin's Maximum Principle and the Lagrange method are used in designing the current and speed controllers respectively. The current controller generates control signals as linear-parametric functions through the offline solving of the quadratic-linear cost function. Instead of using conventional PI controllers in the speed control loop, speed controllers are designed based on the regulating kinetic energy of motors. After driving and simplifying the mathematical equations, the proposed method is simulated. Simulation results are compared with Finite Control Set-MPC. These results validate the prompt and accurate performance of proposed controllers in transient and steady states.

KEYWORDS

Mono inverter dual parallel; Kinetic energy; Model predictive control; Pontryagin's maximum principle; Permanent magnet synchronous motor.

1. Introduction

Attempt to control two motors fed by a single converter goes back to the time when researchers tried using an inverter for feeding motors that are installed on each wheelset and even each bogie of the power trains. Subsequently, the Mono-Inverter Dual-Parallel (MIDP) systems were introduced to be applied in high inertia devices with slow speed changes. The year 1977, namely [1], can be marked as the beginning of researches in this field, and now they are being applied in both industrial and traction applications. Figure 1 illustrates the advantage of the MIDP system over the systems where their motors are fed by a separate inverter. As can be seen, the MIDP motors utilize the integrated controller as well as reduce the weight, volume, power electronic devices, and drive cost. Based on studies done so far, the motor drives in the MIDP systems can be categorized into two groups including weighting-based control and model-based control.

*.Corresponding author.
E-mail address: *abbaszadeh@kntu.ac.ir* (K. Abbaszadeh)

There are two approaches in the weighting-based control. The first is the averaged vector control of motors [2-6]. There are problems with this approach such as severe and long fluctuations in the current waveforms and dependency of the calculated commands on the motor type.

The Master-Slave (MS) method is the second approach in which the elimination of fluctuations and maintaining stable performance of motors are the main concerns [7-10]. The method of reduced-order feedback linearization has been used on independent torque control in the MIDP system [11]. Although the designed controller could hardly control the system at the singular point, it could handle the MIDP system under conditions of severe unequal load torques. The methods mentioned above are based on Field-Oriented Control (FOC) method. The Direct Torque Control (DTC) method was used on the MIDP system [12]. Despite it could introduce a new switching lookup table; the complexity in selecting the appropriate voltage vectors from the switching lookup table is one of its drawbacks in the MIDP method. Reference [13] has also presented a DTC method based on the mean control pattern where the lookup table is just used for induction motors. With the advent of powerful microcontrollers, the Model Predictive Control (MPC) method was used in electrical motor drives [14]. Typically, there are two general approaches to controlling the MIDP system using the MPC method. The first approach, called Finite Control Set Model Predictive Control (FCS-MPC), was applied on two PMSM motors and two induction motors in [15-17] and [18-20], respectively. This method uses just six well-known voltage vectors in SVPWM (Space Vector Pulse Wide Modulation) to minimize the cost function. These vectors have the same amplitude with an angle difference of 60 degrees relative to each other[21]. Certainly, the lowest value of the cost function is not obtained by six control signals specially in the transient state. Hence, the Seek and Split Predictive Torque Control (SS-PTC) method used a large number of voltage space vectors [22]. Depending on the present position of the voltage vector, the SS-PTC searches two adjacent sections of the six sections to find the voltage vector that minimizes the cost function. In addition to the fact that the voltage vector that minimizes the cost function may not be in the mentioned sections because of the condition of the motors, it also takes a long time to obtain the desired voltage vector because of frequently checking the cost function. In FCS-MPC method, generally, the obtained voltage vectors do not lead to the absolute minimum value of the cost function, and the system constraints do not affect the control signal determination process. The second approach, with better performance than FCS-MPC, is the Continues Control Set Model Predictive Control (CCS-MPC) method [23]. Perhaps the pioneer of CCS-MPC is the Optimal Torque Predictive Control method [24, 25]. Severe fluctuations in the transient state and tendency of the cost function to a non-zero value are among the problems in this research. Reference [26] used the system constraints to determine control signals. However, the control loop of optimal angle displacement not only prolonged the fluctuations of the control variables but also increased the sensitivity of the method to the motor parameters. According to the background provided, further studies are needed to introduce a method to obtain optimal control signals for MIDP systems.

This paper presents a comprehensive analytical effective method for designing the current controller that could be used in a single PMSM motor or dual-parallel PMSM motors. The transient and steady states of the motors are also considered in designing the controller. In addition, the necessary and sufficient conditions are considered for the controllability of the system at any given time. Since the designed current controller is based on Pontryagin's Maximum Principle, the obtained control signals are linear-parametric functions of the state variables. An effective speed controller is also introduced based on the nominal power and kinetic energy of the motors. By observing the present kinetic energy of the motors and comparing this energy with the amount of kinetic energy at the reference speed, the control signals of the speed loop are adjusted. The produced control signals in both controllers have a closed analytical form of state variables. Thus, the proposed drive technique saves significant computing time and processing memory. This paper is organized as follows. In the first part, the model of two PMSM motors will be obtained in a rotor reference frame. In order to check the validity of the proposed method and its capability in transient conditions, two low-inertial permanent magnet synchronous motors are considered. In the second part, the design method of the speed and current controllers is introduced, and the necessary and sufficient condition for generating control signals is examined. Then, the sensitivity of the designed controllers will be investigated to unwanted changes in the electrical parameters of the motors. In the next section, the simulation results of the proposed controllers along with their analysis are presented and compared with the FCS-MPC. Finally, a conclusion is presented.

2. Drive Structure of MIDP System

Figure 2 shows the cascade structure of the MIDP system with PMSM motors. Instead of a conventional PI controller, the outer loop is a speed controller that generates control signals $(\hat{I}_{qs})$ based on Energy-based Predictive Control (EPC) of motors. This loop also contains two observers that are estimated the load torque of the motors. The inner loop is a current controller that generates the $\hat{V}_{qds}$ control signals in a very short time based on the Predictive Current Control (PCC). According to the generated control signals in the inner loop, the inverter gate signals are issued by the Space Vector Modulation (SVM) method to generate three-phase voltages for parallel motors. It should be noted that the commands of the component-flux currents are set to zero. Indeed, the magnetic flux of each motor is placed on the d-axis of its coordinate system so that each motor is controlled in the FOC method.

2.1. Modelling of two PMSM Motors in MIDP System

The MIDP system propulsion is supplied via two identical surface-mounted PMSM motors, whose electrical equations can be found in the rotor reference frame [27, 28]. Figure 3 shows the rotating dq rotor frame of each motor in the stationary frame and in the unequal load torque conditions. Since the proposed method is generally based on the FOC method, the rotor magnetic flux of each motor $(\psi_f = |\boldsymbol{\psi}_{f1}| = |\boldsymbol{\psi}_{f2}|)$ is located on its d-axis reference system. Certainly, the dq coordinate system of the inverter could not match the coordinate system of the motors in unequal load torques. Therefore, the electrical

equations of the second motor are transferred to the coordinate system of the first motor. Equation 1 has been employed to transfer the electrical equations of the second motor.

$$Y_{qds2}^{r_1}=\begin{bmatrix} cos(\theta') & -sin(\theta') \\ sin(\theta') & cos(\theta') \end{bmatrix} Y_{qds2}^{r_2};\ \ \theta'=\theta_{r1}-\theta_{r2} \qquad (1)$$

where $Y_{qds2}^{r_1}$ is the voltage or current vector of the second motor in the first motor dq coordinate system, and $Y_{qds2}^{r_2}$ is the voltage or current vector of the second motor in its own dq coordinate system. The electrical angle displacements of the motors are θ_{r1} and θ_{r2}, respectively. It should be noted that the electrical angle difference, θ', is not zero in unequal load torque conditions, and its value depends on unbalancing in the load torques. Since this electrical angle is a stability criterion of the PMSMs, this angle should not exceed $\frac{\pi}{2}$ degrees. The electrical equations of both motors in the dq coordinate system of the first motor are as follows:

$$\begin{cases} I_{qs2}^{\bullet r_1}(t)=\frac{1}{L}V_{qs2}^{r_1}(t)-\frac{r_s}{L}I_{qs2}^{r_1}(t)-\omega_{r1}(t)I_{ds2}^{r_1}(t)-\dots \\ \qquad \dots-\frac{1}{L}\omega_{r2}(t)\psi_f cos(\theta'); \\ I_{ds2}^{\bullet r_1}(t)=\frac{1}{L}V_{ds2}^{r_1}(t)-\frac{r_s}{L}I_{ds2}^{r_1}(t)+\omega_{r1}(t)I_{qs2}^{r_1}(t)-\dots \\ \qquad \dots-\frac{1}{L}\omega_{r2}(t)\psi_f sin(\theta'); \end{cases} \qquad (2)$$

According to the electrical equations of the first motor, the compact form of the electrical equations of both motors can be written as follows:

$$X^{\bullet}(t)=f\left(X(t),\Theta(t),t\right)=A_M X(t)+B_M\Theta(t)+D_M(t); \qquad (3)$$

$$\begin{cases} X^{\bullet}(t)=[\,I_{qds1}^{\bullet r_1}(t)\ \ I_{qds2}^{\bullet r_1}(t)\,]^T;\ X(t)=\left[I_{qds1}^{r_1}(t)\ \ I_{qds2}^{r_1}(t)\right]^T; \\ \Theta(t)=\left[V_{qs}^{r_1}(t)\ \ V_{ds}^{r_1}(t)\right]^T; \qquad D_M(t)=\left[\Delta_1\ \ \Delta_2\right]^T; \\ A_M=\begin{bmatrix}\gamma_{11} & \gamma_{12}\\ \gamma_{21} & \gamma_{22}\end{bmatrix}; \qquad B_M=\frac{1}{L}\begin{bmatrix}1 & 0 & 1 & 0\\ 0 & 1 & 0 & 1\end{bmatrix}^T; \end{cases}$$

where γ_{12} can be found in Appendix. Since both motors are fed by a three-phase inverter, the vector of control signals is 2×1. Therefore, it could assume that $V_{qs}^{r1}=V_{qs1}^{r1}=V_{qs2}^{r1}$ and $V_{ds}^{r1}=V_{ds1}^{r1}=V_{ds2}^{r1}$.

3. Designing the Outer Loop Controller of the MIDP System

This section deals with the design of the outer loop controller that is regulated the speed of the motors by $\hat{I}_{qs1}^{r_1}$ and $\hat{I}_{qs2}^{r_1}$. Indeed, the control signals of the $\hat{I}_{qs1}^{r_1}$ and $\hat{I}_{qs2}^{r_1}$, known as the torque-component currents, are the command signals of the inner loop. In the following, the design of each of them is explained.

3.1. MPC-Based Speed Controller Design

With the least fluctuation and in the shortest possible time, the motor speeds reach the reference speed when the designed speed controller adjusts the commands of the torque-component currents in the inner loop. Accordingly, the performance index is defined as follows:

$$\mathcal{J}=\min_X\left\{\frac{1}{2}\int_{t_i}^{t_f}\left(\hat{X}-X(\tau)\right)^T Q_{sw}(\tau)\left(\hat{X}-X(\tau)\right)d\tau\right\}; \qquad (4)$$

$$\begin{cases} X(t)=\left[\omega_{r_1}(t)\quad \xi_{k_1}(t)\quad \omega_{r_2}(t)\quad \xi_{k_2}(t)\right]^T; \\ \hat{X}=\left[0\quad \frac{1}{2}J_t\hat{\omega}_{r_1}^{\,2}\quad 0\quad \frac{1}{2}J_t\hat{\omega}_{r_2}^{\,2}\right]^T; \end{cases}$$

where the $X(t)$ state vector contains the angular accelerations $\left(\omega_r^{\bullet}(t)\right)$ and the kinetic energies $\left(\xi_k(t)\right)$. The total inertia moment of the load and motor is J_t, and $Q_{sw}(t)$ is the deterministic positive weighting matrix. By replacing the state and reference vectors in the performance index and minimizing the integral cost function relative to the motor speed slopes, Equation 5 is obtained.

$$\begin{cases} \omega^{\bullet}_{r_1}(t)=\dfrac{2J_t}{p^2}\left(\dfrac{Q_{sw_{12}}(t)+Q_{sw_{21}}(t)}{Q_{sw_{11}}}\right)\left(\hat{\omega}_{r_1}{}^2-\omega_{r_1}(t_i)^2\right); \\ \omega^{\bullet}_{r_2}(t)=\dfrac{2J_t}{p^2}\left(\dfrac{Q_{sw_{34}}(t)+Q_{sw_{43}}(t)}{Q_{sw_{33}}}\right)\left(\hat{\omega}_{r_2}{}^2-\omega_{r_2}(t_i)^2\right); \end{cases} \quad (5)$$

The reference and electrical angular speeds of the motors at t_i are $\hat{\omega}_{r_1},\hat{\omega}_{r_2},\omega_{r_1}(t_i),\omega_{r_2}(t_i)$, respectively. Elements of the $Q_{sw}(t)$ weighting matrix can be selected based on the kinetic energy required by the motors to track the speed command or change the speed feedback. If the electrical energy required to change the speed in Δt period is expressed as follows:

$$W_e(t_i)=\frac{2}{p}\left(\omega_r(t_i+\Delta t)-\omega_r(t_i)\right)T_L(t_i)\Delta t=\frac{2}{p}\omega_r(t)T_L(t_i)\Delta t^2; \quad (6)$$

where Δt is assumed smaller than the electrical time constant of motors and the load torque is assumed constant in this period. Since this energy leads to a speed change in the Δt period, it can be equated with the kinetic energy required to change speed. The result of this selection is as follows:

$$W_e(t_i)=\Delta E_c=\frac{2J_t}{p^2}\left(\left(\hat{\omega}_r\right)^2-\left(\omega_r(t_i)\right)^2\right); \quad (7)$$

Elements of the $Q_{sw}(t)$ weight matrix are obtained by comparing Equation 5 with Equation 7 as follows:

$$\begin{cases} Q_{sw_{11}}=Q_{sw_{33}}=\dfrac{2}{p}\Delta t^2; \\ Q_{sw_{12}}(t)=Q_{sw_{21}}(t)=\dfrac{1}{2T_{L_1}(t_i)}; \\ Q_{sw_{34}}(t)=Q_{sw_{43}}(t)=\dfrac{1}{2T_{L_2}(t_i)}; \end{cases}$$

By choosing an arbitrary value for $Q_{sw_{22}}$ and $Q_{sw_{44}}$, to keep the matrix $Q_{sw}(t)$ as positive deterministic, and using the mechanical equation of PMSM motors, the commands of the torque-component currents are as follows:

$$\hat{I}^{r_1}_{qsk}(t_i)=\frac{8J.J_t}{\Delta t^2 3p\psi_f T_{L_k}(t_i)}\left(\left(\hat{\omega}_{r_k}\right)^2-\left(\omega_{r_k}(t_i)\right)^2\right)+\frac{8B_m}{3p^2\psi_f}\omega_{r_k}(t_i) + \frac{4}{3p\psi_f}T_{L_k}(t_i); \quad (8)$$

where $T_{L_k}(t_i)$ is the load torque of the kth motor at t_i. The $T_L(t_i)$ equation can be written, using the backward Euler approximation, as follows [29]:

$$T_L(t_i)=\frac{3}{2}\frac{p}{2}\psi_f I^r_{qs}(t_i)-J\frac{2}{p}\left(\frac{\omega_r(t_i)-\omega_r(t_{i-1})}{\tau_p}\right)-B_m\frac{2}{p}\omega_r(t_i); \quad (9)$$

To increase the accuracy of the calculated value, the value of load torque is set equal to the average of the last 10 samples. Since the balance between the required energy and the kinetic energy on the motor shaft play an important role in the generation of control signals, this method of speed control can be introduced as Energy-based Predictive Control (EPC). When the $\hat{\omega}_{r_k}$ is issued, the kinetic energy difference appears. If the energy flowed to the motor shaft is greater than the kinetic energy difference, the motor reaches a speed more than the reference speed in transient mode, and vice versa. If the energy delivered to the motor is equal to the kinetic energy difference, no excess energy will be injected into the motor. Therefore, the energy that causes the speed fluctuations will not inject into the motor. When the motor speed approaches the reference speed, the kinetic energy difference will be reduced, and the energy delivered to the motor for the desired changes is reduced. Equation 9 suggests when the speed changes of each motor are in such a way that each of the $\hat{I}^{r_1}_{qs1}(t_i)$ and $\hat{I}^{r_1}_{qs2}(t_i)$ commands exceeds the nominal current limits, the nominal current value of the motors must replace with the calculated command. It is necessary to mention that this controller can use in any electrical smooth-pole motor.

4. Designing Inner Loop Controller Based on Pontryagin's Maximum Principle

The inner loop control variables are adjusted through the MPC method. Since adjusting four control variables is complicated with two control signals, and the control variable dynamics is also being fast in the inner loop relative to the other loop, these make complicate the solving of the cost function. Therefore, the design of the controller according to Pontryagin's Maximum Principle (PMP) is proposed. To bring the system with Equation 3 to the desired conditions, the performance index of the MPC problem is considered as follows:

$$\mathcal{J}=Min\frac{1}{2}\Big[\big(X(t_f)-\hat{X}\big)^T Q_f\big(X(t_f)-\hat{X}\big)+\cdots \\ \cdots+\int_{t_i}^{t_f}\big(X(t)-\hat{X}\big)^T Q\big(X(t)-\hat{X}\big)+\Theta^T(t)R\Theta(t)d\tau\Big]; \quad (10)$$

where $Q=0, Q_f \geq 0$ and $R>0$ are weighting matrices to be selected, $\hat{X}$ is the reference state vector, X is the optimal value of the state vector, t_f is the end of the predictive horizon, and $X(t_f)$ is the state vector at t_f. For solving Equation 10, the Pontryagin's function is written as follows [30-33]:

$$\mathcal{H}=Z\big(X(t),\hat{X},t\big)+\psi^T(t)\big(f\big(X(t),\Theta(t),t\big)\big); \quad (11)$$

where $\psi(t)$ is the quasi-variable state vector with equal dimension to the state vector $X(t)$, and $Z\big(X(t),\hat{X},t\big)$ is the second statement of Equation 14. Based on the PMP, necessary conditions for optimality are $X(t)=\frac{\partial\mathcal{H}}{\partial\psi}, \psi(t)=-\frac{\partial\mathcal{H}}{\partial X}$ and $\frac{\partial\mathcal{H}}{\partial\Theta}=0$. The linear equation of the controlled system and the necessary conditions of optimality make it possible to write the differential equations as follows [34]:

$$\begin{cases} X^{\bullet}(t)=A\big(X(t_i)\big)X(t)+B\Theta(t)+D\big(X(t_i),t_i\big); \\ \psi^{\bullet}(t)=-Q\big(X(t)-\hat{X}\big)-A^T\big(X(t_i)\big)\psi(t); \\ X(t_i)=X_{t_i}; \\ \psi(t_f)=\frac{\partial}{\partial X(t)}\Big(\big(X(t_f)-\hat{X}\big)^T Q_f\big(X(t_f)-\hat{X}\big)\Big)\Big|_{t_f}= \\ \qquad\qquad Q_f\big(X(t_f)-\hat{X}\big); \end{cases} \quad (12)$$

After using the forward Euler method to approximate the left side of Equation 12, calculating the predicted value of the state vector at the end of the sampling interval, and also calculating the value of the quasi-state variable at the beginning of the sampling interval, $\psi(t_i)$ can be written as follows:

$$\psi(t_i)=A'_{\psi}X(t_i)+B'_{\psi}\Theta_{\psi}+D'; \quad (13)$$

where Θ_{ψ} is the reference vector of the control signals in sampling period. The calculations related to the coefficients A'_{ψ}, B'_{ψ} and D'_{ψ} can also be found in the appendix. Thus, having $\psi(t_i)$ the control signals are obtained as follows:

$$\begin{cases} \Theta(t_i)=\alpha(t_i)X(t_i)+\beta(t_i)\Theta_{\psi}+\delta(t_i); \\ \alpha(t_i)=-R^{-1}B^T A'_{\psi};\ \beta(t_i)=-R^{-1}B^T B'_{\psi}; \\ \delta(t_i)=-R^{-1}B^T D'_{\psi}; \end{cases} \quad (14)$$

As it can be seen in Equation 14, the control signals are obtained as linear-parametric functions from the measurable state variables. As a result, the computing time of the control signals reduces significantly.

4.1. Designing Current Controller in MIDP System with Two PMSM Motors

According to the controller design process, the required vectors and matrices are defined as follow:

$$X(t)=\Big[I_{qs1}^{r_1}(t)\quad I_{ds1}^{r_1}(t)\quad I_{qs2}^{r_1}(t)\quad I_{ds2}^{r_1}(t)\Big]^T$$
$$\hat{X}=\Big[\hat{I}_{qs1}^{r_1}(t)\quad \hat{I}_{ds1}^{r_1}(t)\quad \hat{I}_{qs2}^{r_1}(t)\quad \hat{I}_{ds2}^{r_1}(t)\Big]^T;$$
$$\Theta(t)=\Big[V_{qs}^{r_1}(t)\quad V_{ds}^{r_1}(t)\Big]^T;\ R=\begin{bmatrix} R_{11} & 0 \\ 0 & R_{22} \end{bmatrix}; R_{11}=R_{22};$$

The elements of the R diagonal matrix must be considered equal in order to prevent prejudging the control signals. The Q and Q_f are the 4×4 diagonal matrices of the deterministic positive. After defining the required vectors and matrices, the control signals can be calculated by having A'_{ψ}, B'_{ψ} and D'_{ψ} matrices in Equation 14. Based on the obtained relationships for them, the matrices are as follows:

$$A'_{\psi_4}=\tau_p^2 c_1\begin{bmatrix} -Q_{f2} & 0 & Q_{f2} & 0 \\ 0 & -Q_{f1} & 0 & Q_{f1} \\ Q_{f2} & 0 & -Q_{f2} & 0 \\ 0 & Q_{f1} & 0 & -Q_{f1} \end{bmatrix};$$

$$A'_{\psi_3}=\begin{bmatrix} 0 & a'_{\psi_{3,1}}-a'_{\psi_{3,3}} & 0 & -a'_{\psi_{3,1}}-a'_{\psi_{3,3}} \\ a'_{\psi_{3,3}}-a'_{\psi_{3,2}} & 0 & a'_{\psi_{3,3}}+a'_{\psi_{3,2}} & 0 \\ 0 & -a'_{\psi_{3,1}}-a'_{\psi_{3,3}} & 0 & a'_{\psi_{3,1}}-a'_{\psi_{3,3}} \\ a'_{\psi_{3,3}}+a'_{\psi_{3,2}} & 0 & a'_{\psi_{3,3}}-a'_{\psi_{3,2}} & 0 \end{bmatrix};$$

$$A'_{\psi_2}=\begin{bmatrix} a'_{\psi_{2,1}} & 0 & a'_{\psi_{2,2}} & 0 \\ 0 & a'_{\psi_{2,3}} & 0 & a'_{\psi_{2,4}} \\ a'_{\psi_{2,2}} & 0 & a'_{\psi_{2,1}} & 0 \\ 0 & a'_{\psi_{2,4}} & 0 & a'_{\psi_{2,3}} \end{bmatrix};$$

$$A'_{\psi_1}=\begin{bmatrix} 0 & a'_{\psi_{1,2}} & 0 & a'_{\psi_{1,4}} \\ a'_{\psi_{2,1}} & 0 & a'_{\psi_{2,3}} & 0 \\ 0 & a'_{\psi_{1,4}} & 0 & a'_{\psi_{1,2}} \\ a'_{\psi_{2,3}} & 0 & a'_{\psi_{2,1}} & 0 \end{bmatrix};$$

$$A'_{\psi_0}=\upsilon_5\mu\begin{bmatrix} -A_{11}v_1 & 0 & -A_{13}v_1 & 0 \\ 0 & -A_{22}v_2 & 0 & -A_{24}v_2 \\ -A_{13}v_1 & 0 & -A_{11}v_1 & 0 \\ 0 & -A_{24}v_2 & 0 & -A_{22}v_2 \end{bmatrix};$$

$$B'_{\psi_3}=\tau_p c_1\begin{bmatrix} 0 & -Q_{f2} & 0 & Q_{f2} \\ Q_{f1} & 0 & -Q_{f1} & 0 \\ 0 & Q_{f2} & 0 & -Q_{f2} \\ -Q_{f1} & 0 & Q_{f1} & 0 \end{bmatrix};$$

$$B'_{\psi_2}=\begin{bmatrix} b'_{\psi_{0,3}} & 0 & b'_{\psi_{0,5}} & 0 \\ 0 & b'_{\psi_{0,4}} & 0 & b'_{\psi_{0,6}} \\ b'_{\psi_{0,5}} & 0 & b'_{\psi_{0,3}} & 0 \\ 0 & b'_{\psi_{0,6}} & 0 & b'_{\psi_{0,4}} \end{bmatrix};$$

$$B'_{\psi_1}=\begin{bmatrix} 0 & b'_{\psi_{1,2}} & 0 & b'_{\psi_{1,4}} \\ b'_{\psi_{1,3}} & 0 & b'_{\psi_{1,5}} & 0 \\ 0 & b'_{\psi_{1,4}} & 0 & b'_{\psi_{1,2}} \\ b'_{\psi_{1,5}} & 0 & b'_{\psi_{1,3}} & 0 \end{bmatrix};$$

$$B'_{\psi_0}=\begin{bmatrix} A_{11}b'_{\psi_{0,1}} & 0 & A_{13}b'_{\psi_{0,1}} & 0 \\ 0 & A_{22}b'_{\psi_{0,2}} & 0 & A_{24}b'_{\psi_{0,2}} \\ A_{13}b'_{\psi_{0,1}} & 0 & A_{11}b'_{\psi_{0,1}} & 0 \\ 0 & A_{24}b'_{\psi_{0,2}} & 0 & A_{22}b'_{\psi_{0,2}} \end{bmatrix};$$

$$\begin{cases} A'_{\psi}=\dfrac{-0.5c_1^{-1}}{\left(\omega_{r_1}^2-\sigma^2\right)}\left(A'_{\psi_4}\omega_{r_1}^4+A'_{\psi_3}\omega_{r_1}^3+A'_{\psi_2}\omega_{r_1}^2+A'_{\psi_1}\omega_{r_1}+A'_{\psi_0}\right); \\ B'_{\psi}=\dfrac{0.5c_1^{-1}}{\left(\omega_{r_1}^2-\sigma^2\right)}\left(B'_{\psi_3}\omega_{r_1}^3+B'_{\psi_2}\omega_{r_1}^2+B'_{\psi_1}\omega_{r_1}+B'_{\psi_0}\right); \\ D'_{\psi}=-\tau_p B'_{\psi}D_M; \end{cases}$$

(15)

Each of the cofactors can be found in the appendix. Notice that all the obtained matrices will be fixed matrices once the MIDP motors have been specified and the weighting matrices have been selected. As a result, by performing simple calculations and spending a short time, α, β, and δ are obtained as functions of the speed and position of the motors. Indeed, if one pays attention to Equation 14, α, β, and δ are obtained by using 104 multiplication operators and 132 addition operators. Although the generation process of control signals by Equation 14 is fast and easy, the controllability of the inner loop depends on the availability of the A'_{ψ} and B'_{ψ} matrices at each sampling time. Therefore, the denominator in these matrices must be opposite to zero. By instituting the parameters, the denominator expression becomes as follows:

$$\omega_{r_1}^2+\frac{L^2R_{11}\left(2\tau_p^2\left(Q_1-Q_{f1}\mu\right)+L^2R_{11}\right)\left(2\tau_p^2\left(Q_2-Q_{f2}\mu\right)+L^2R_{11}\right)}{4\tau_p^4Q_{f1}Q_{f2}};$$

When the μ value is chosen negative, the second statement of the denominator expression is positive value. Therefore, the denominator expression will be positive and non-zero. According to $\mu=\left(r_s/L-1/\tau_p\right)$, it is assumed that the τ_p value is definitely smaller than the electrical time constant of the motors.

5. Simulation results

To show the performance and capability of the proposed controller, MATLAB/Simulink software is used to run the proposed drive technique. Because low-inertia motors have fast dynamics, selecting such a motor can be a major challenge for controllers to generate control signals. Hence, two identical PMSM motors manufactured by LS Company with XML-SB04A series are chosen as MIDP system motors. The specifications are listed in Table 1. The specifications of the SVM modulation inverter used are listed in Table 2. Based on section 4, the internal and external loop controller values should be determined. In the design of the inner loop controller, the value $\tau_p = 0.125\times10^{-3}$ and the weighting matrices are selected as follows:

$$Q_f=\begin{bmatrix} 280 & 0 & 0 & 0 \\ 0 & 5800 & 0 & 0 \\ 0 & 0 & 280 & 0 \\ 0 & 0 & 0 & 5800 \end{bmatrix};\quad Q=\begin{bmatrix} 15 & 0 & 0 & 0 \\ 0 & 85 & 0 & 0 \\ 0 & 0 & 15 & 0 \\ 0 & 0 & 0 & 85 \end{bmatrix};$$

$$R=\begin{bmatrix} 1 & 0 \\ 0 & 1 \end{bmatrix};$$

In EPC speed controller, $\Delta t = 0.0118$ and the sampling frequency of the motor feedback signals is assumed to be 25^{KHz} .

5.1. Comparison between the presented method and the FCS-MPC

According to Figure 4, the outer loop of FCS-MPC structure uses conventional PI controllers and the cost function according to Equation 16 is evaluated by six control signals in the inner loop.

$$CF = Min\sum_{j=1}^{2}\left[K_{\psi_j}\left|\hat{I}_{ds_j}-I_{ds_j}^{r_1}\right|^2+K_{T_j}\left|\hat{I}_{qs_j}-I_{qs_j}^{r_1}\right|^2\right]; \qquad (16)$$

where $\hat{I}_{qs}$ are the reference control signals obtained from Equation 9 and $\hat{I}_{ds}=0$. This method is characterized by the simplicity of the design process, no need for voltage modulators, online optimization, variable switching frequency and the inclusion of system constraints. To produce control signals must also be performed 342 multiplication and 168 addition operations. However, with six voltage vectors, the comprehensive minimum value of the cost function cannot be obtained. In what follows, the performance of the FCS-MPC method and the proposed method are compared in diverse control modes.

5.1.1. Startup stage

Motors are started up with nominal speed and 50% of nominal speed. In this strategy, the load torque of the first motor is always in the nominal value, but the load torque of the second motor varies between the nominal value and 70% of the nominal value. Figure 5a to 5d are related to proposed method so that both motors have nominal torque in Figure 5a and Figure 5c, but the second motor, Figure 5b and Figure 5d, has 70% of first motor torque. In the same order, Figure 5e to 5h are related to FCS-MPC. The result obtained in Figure 5 shows that the proposed method in all starting modes has been able to reach the speed of the motors to the reference speed in less settling time and lower speed ripple than the FCS-MPC and even without offset error. Comparing Figure 5b with 5F illustrates that the FCS-MPC method controls only one motor in start-up mode and has no control over the other motor, while the proposed MPC is able to handle both motors in this stage. Another prominent feature of the proposed method is the relative independence of the settling time from changes in the speed and load torque commands. As can be seen, the settling time in Figures 5a to 5d is around 0.025 seconds, while this time varies in Figures 5e to 5h for the FCS-MPC method.

5.1.2 Diverse operating conditions

Figure 6a illustrates the speed command and the load torques as per unit. The rated values of the motors are selected as the base values. The motors operate at 50 percent of the rated speed and 70 percent of the rated load torques under balanced loading conditions. In 0.05 seconds, the mechanical loads are unbalanced so that the load torque of the first motor changes to the nominal value, and the load torque of the second motor changes to 40% of the nominal torque. In 0.15 seconds, the speed command reaches the nominal value with the rate of 25 per unit per second in unbalanced load conditions of motors. Then, it decreases abruptly to 1000 r.p.m (33% of the rated value) in 0.3 seconds. At last, the speed command and the second motor load torque change in step to their rated values in 0.4 seconds. Figure 6a shows the performance of both methods in tracking the reference speed. As seen in Figure 6b in 0.05 seconds, the proposed method has been able to pass the transient state in a short period with low fluctuations and to track the reference speed well in the steady-state without occurrence pendulum mode. However, in Figure 6c, the motors controlled by the FCS-MPC method have been able to track the reference speed by fluctuating. Even the damping rate of the fluctuations is so low that they are also seen in tracking the reference speed with a constant slope. As a result, when the unbalancing in load torques has been reached 0.6 per unit, the proposed method can control both motors agreeably than the other method. The torque waveforms also confirm that the torque ripple in the

proposed method is much lower than the FCS-MPC method in this interval (Figure 7). The control performance of both methods is suitable in tracking reference speed at the second strategy (from 0.15 to 0.3 seconds).
The remarkable feature of the proposed control method is visible in 0.3 seconds. The speed command of the motors is suddenly reduced to 33.3% of the rated value while the load torques are unequal. The approach of any control method in such conditions is to use the braking torque to reduce speed. The speed waveforms in the proposed method have tracked the new speed command in transient and steady states without fluctuation, and the torque waveforms without overshoot have returned to their previous values after the breaking stage (Figure 6b and 8a). However, the FCS-MPC method has not operated acceptably at this stage because the speed of the motors had a considerable deviation (over than 800 rpm) from the command speed in the transient state, and the torque waveforms have returned to their previous values with a significant overshoot. The speed waveforms in a steady-state are also accompanied by severe fluctuations, which may cause instability in the control process (Figure 6c and 8b). Regarding the dynamic performance of the FCS-MPC controllers within the interval, the transient state fluctuations can be attributed to the excess energy imposed on motors. However, in the proposed method, the new reference speed value is taken into account in the prediction horizon of the external loop controller. Therefore, from the very beginning, it applies the required braking torque to the motors, and the amount of braking torque decreases as the motor speeds approach the reference value. Consequently, no excess energy is applied to two motor shafts. As shown in Figure 6b, when the speed decreases, the braking torque also decreases. Similarly, when the electromagnetic torques are equal to the load torques, the speed of the motors reaches the reference value with no fluctuation in the electromagnetic torques (Figure 7a). The controller behaves in such a way that the transient state passes and reaches a stable value without any fluctuations in speed and torque. By applying the rated load torques to the motors and issuing the rated speed command in the last section of the control strategy, both methods have a good performance in tracking the speed and controlling load torques. However, the torque and current waveforms in the FCS-MPC method have more ripple than the proposed method. A comparison of the torque waveforms in Figures 8a and 8b shows that the torque ripple is less in the proposed method than the FCS-MPC method.
The current waveform of the motors confirms the existence of more ripples in the FCS-MPC method than the proposed method (Figure 8). As can be seen, Figure 8b has more noise than Figure 8a in both balanced and unbalanced load conditions. To compare the amount of the produced ripple on two methods, Figure 9 shows the harmonic profiles of the phase-a currents of the motors. The current harmonic profiles are obtained while the motors are rotating at quarter of rated speed as well as the first motor is at rated load torque and the second motor is at 70% of rated load torque. According to the harmonic profile, the current amplitude of the fundamental harmonic is almost the same on both methods. However, the THD of the motor currents on the proposed method is approximately half THD on the FCS-MPC method.

5.1.3. Comparing the cost function value in two methods

According to the strategy used in Figure 6, the cost function value is obtained by calculating Equation 16 in the proposed MPC and FCS-MPC methods. As seen in Figure 10, the cost function values are approximately equal under balanced load torque conditions, even at half the nominal speed. When the load torques of the MIDP system are unbalanced, the performance of the FCS-MPC method is dependent on the speed command, so that the cost function value in this method fluctuates at asynchronous speeds, and its value is about zero at synchronous speed. Also, the cost function value in this method has increased significantly with a sudden decrease in speed in 0.03 seconds. As a result, no optimal control is applied to the MIDP system. The cost function value in the proposed MPC method, unlike the FCS-MPC method, is about zero over unbalanced torque conditions and is almost independent of the speed command. Even at 0.03 seconds, the small value of the cost function indicates the realization of the optimal control process in the MIDP system. According to the results presented in section 5.1, Table 3 compares the proposed method with the FCS-MPC method. As can be seen, fewer mathematical operations, simultaneous control of two parallel motors, fixed switching frequency, and the optimal response of the torque, current, and speed are among the advantages of the proposed method.

5.2. Impact of EPC on MIDP System

The speed controller depends on the system model and the mechanical equation of rotational motion. The system model term actually refers to the motor torques that are just electromagnetic torque because of the equality stator inductances in smooth-pole machines. Since the mechanical equation of rotational motion can use in any electric motor, the presented speed controller can use in any smooth-pole electric machine. Despite this capability, EPC performance is compared with conventional PI controllers to perceive its impact on MIDP systems. Therefore, the two PI controllers in the outer loop of Figure 2 are replaced by the EPC speed controller. Figure 11 shows the speed error of both controllers. The speed error equation is as follows:

$$E_{\omega}=\left|\omega_{ref}-\omega_{r,k}\right|; \qquad k=1,2 \tag{17}$$

Before 0.05 seconds, the motors had been rotating at nominal speed and nominal load torques. In 0.05 seconds, the load torque of the second motor is reduced by 30%. At 0.1 seconds, the speed command is reduced by 50%, while motors have unequal load torques. Comparing Figure 11a and Figure 12c illustrate the lower amplitude of speed error in the EPC controller than the PI controller. The approximate equality of the speed error in Figure 11a indicates that the EPC controller pays attention to the dynamics of both motors. However, the large difference in E_{ω} amplitude in Figure 11c indicates that the PI controller pays attention to only one of the motors. In the speed change stage (Figure 11b and 11d), both speed controllers

must brake to reduce speed. Therefore, 150 rpm speed error is a normal process. Although Figure 11b does not show the speed overshot after braking, the overshot is approximately seen at about 50 rpm on both motors in Figure 11d. Comparing the results of the two controllers indicates that both of them generally have the same response in steady-state, however, the transient response of the EPC controller has much fewer speed fluctuations than the PI speed controller. As a result, the EPC controller may be efficient in reducing the fatigue phenomena and in increasing the motor shaft life.

5.3. Stability and Sensitivity Evaluation of the Proposed Control Method

5.3.1. The Stability Maintaining of the PMSM Motors

The stability maintaining of the electrical motors after the controllability is an important subject in the electrical motor drives. The stability problem in induction motors that are previously used in the MIDP system is not so important because of having the short-circuited rotor winding and the slip coefficient. However, the PMSM motors are more commonly used in the MIDP systems today, and their stability maintenance is an important challenge in their use [35]. As mentioned in [36], the eigenvalues of the system state matrix in steady-state could determine the stability status of the MIDP system with the PMSM motors.

However, it is difficult to obtain the analytical expression of the eigenvalues. Therefore, the locus of the state matrix eigenvalues is checked for the certain load torques relative to the left half of the Cartesian coordinate system. In [37], the study of the angle difference between the two rotors in the two PMSMs was introduced as a criterion of stability.

According to this, the slope or the percentage of the load torque changes must be such that the angle difference among rotors does not oscillate and does not exceed 90 degrees. In this section, the angle difference (θ') between the rotors is examined to evaluate the stability. Two strategies have been applied in this subject that illustrated in Figure 12a and Figure 12b. As seen in Figure 12c and Figure 12d, the electrical angle difference between the two rotors has remained constant in steady-state conditions. Therefore, the stability of the PMSM motors is ensured in the range of load torque changes.

5.3.2 The Sensitivity Analysis of the Proposed Control Method

In a MIDP system, the parameters of both motors might be not identical because of inaccuracy in construction, temperature effects, and operating conditions. Therefore, in Figure 13, the change effect of the stator resistor, inductance, and linkage flux is considered on the performance of the designed controllers. In order to study sensitivity analysis, both motors are rotated at rated speed, and the parameter values only in the first motor are changed step by step from -%25 to +%50. As illustrated in Figure 13a and 15b, the designed controllers can correctly operate without considering the variation of R_s (stator resistor) and L_s (stator inductance) even in unequal load torques. Figure 13c is also shown that the sensitivity of the controllers is very insignificant when the flux linkage changes in range ±%10.

6. Conclusion

Feeding two parallel motors with a single inverter can significantly reduce the volume, weight, and drive cost. Major challenges confronted by the MIDP systems are:

- Occurring pendulum mode in the condition that the load torque of motors is unbalanced.
- Four control variables related to the current controller must be able to track their reference values with just two control signals.
- The control signal in speed and current controllers should be calculated quickly due to the fast dynamics of the motors.

This paper has introduced the kinetic energy-based speed controller as an alternative to conventional PI controllers. This controller can considerably reduce the fluctuations caused by load torque imbalance. It has also been able to prevent pendulum mode in the high imbalance of load torques. Since this controller is designed considering the motor's kinetic energy, it does not impose excess energy on them in changing the speed command. As a result, it does not cause fluctuations in motor speed that the shaft fatigue has appeared on motors.

On the other hand, the control signals in the current controller have a closed form so that the computational volume of its control signals is less than the FCS-MPC method, which is known as the fastest method of the model predictive control. The introduced current controller also evaluates the entire voltage space vector to produce control signals that lead to optimal system performance.

The optimal performance of the proposed MPC is clearly observed by comparing its THD value and cost function to the FCS-MPC method. Stability evaluation also confirmed that even in the severe imbalance of the load torques, the pendulum mode does not occur in motors and the proposed controllers have high reliability. Finally, the sensitivity evaluation to changing electrical parameters shows that if the unwanted change in parameters is less than 10%, the performance of the controllers will still be efficient.

Appendix

$$\gamma_{11}=\gamma_{22}=\begin{bmatrix} -\frac{r_s}{L} & -\omega_{r1}(t) \\ \omega_{r1}(t) & -\frac{r_s}{L} \end{bmatrix};\ \Delta_1=\frac{\psi_f}{L}\begin{bmatrix} -\omega_{r1}(t) \\ 0 \end{bmatrix};$$

$$\Delta_2=-\frac{\psi_f}{L}\omega_{r2}(t)\begin{bmatrix} cos(\theta') \\ sin(\theta') \end{bmatrix};$$

Calculation $\Theta(t_i)$ in Equation 20 had parameters that are defined as follows:

$$\mu=\left(\frac{r_s}{L}-\frac{1}{\tau_p}\right); \qquad \upsilon_1=\tau_p^2\left(Q_1-Q_{f1}\mu\right); \qquad \upsilon_3=\tau_p^2 Q_{f1};$$

$$a_1=\frac{v_1}{L^2R_{11}}; \qquad \upsilon_2=\tau_p^2\left(Q_2-Q_{f2}\mu\right); \qquad \upsilon_4=\tau_p^2 Q_{f2};$$

$$a_2=\frac{v_2}{L^2R_{11}}; \qquad c_1=2b_1b_2; \qquad \upsilon_5=\tau_p^2\mu;$$

$$b_1=\frac{v_4}{L^2R_{11}}; \qquad b_2=-\frac{v_3}{L^2R_{11}}; \qquad b'_{\psi_{0,1}}=\frac{v_1}{\tau_p};$$

$$b'_{\psi_{0,2}}=\frac{v_2}{\tau_p}; \qquad \sigma^2=\frac{(2a_1+1)(2a_2+1)}{2c_1};$$

$$b'_{\psi_{0,3}}=-\tau_p Q_{f2}b_2-c_1b'_{\psi_{0,1}}; \qquad b'_{\psi_{0,4}}=\tau_p Q_{f1}b_1-c_1b'_{\psi_{0,2}};$$

$$b'_{\psi_{0,5}}=-\tau_p Q_{f2}b_2+c_1b'_{\psi_{0,1}}; \qquad b'_{\psi_{0,6}}=\tau_p Q_{f1}b_1+c_1b'_{\psi_{0,2}};$$

$$b'_{\psi_{1,2}}=\tau_p A_{22}Q_{f2}-b_1b'_{\psi_{0,1}}; \qquad b'_{\psi_{1,4}}=\tau_p A_{24}Q_{f2}-b_1b'_{\psi_{0,1}};$$

$$b'_{\psi_{1,3}}=-\tau_p A_{11}Q_{f1}-b_2b'_{\psi_{0,2}}; \qquad b'_{\psi_{1,5}}=-\tau_p A_{13}Q_{f1}-b_2b'_{\psi_{0,2}};$$

$$A_{11}=(a_1+1)(2a_2+1); \qquad A_{13}=-a_1(2a_2+1);$$

$$A_{24}=-a_2(2a_1+1); \qquad A_{22}=(a_2+1)(2a_1+1);$$

$$a'_{\psi_{3,1}}=\tau_p^2c_1\left(Q_1+\left(Q_{f2}-Q_{f1}\right)\mu\right);$$

$$a'_{\psi_{3,2}}=\tau_p^2c_1\left(Q_2+\left(Q_{f1}-Q_{f2}\right)\mu\right);$$

$$a'_{\psi_{3,3}}=\frac{\upsilon_3\upsilon_4}{L^2R_{11}};$$

$$a'_{\psi_{2,1}}=\tau_p^2\mu\left(c_1\left(Q_1-Q_{f1}\mu\right)+Q_{f2}b_2\right)-\tau_p^2\left(b_1\left(Q_1-Q_{f1}\mu\right)-A_{22}Q_{f2}\right);$$

$$a'_{\psi_{2,2}}=-\tau_p^2\mu\left(c_1\left(Q_1-Q_{f1}\mu\right)-Q_{f2}b_2\right)-\tau_p^2\left(b_1\left(Q_1-Q_{f1}\mu\right)-A_{24}Q_{f2}\right);$$

$$a'_{\psi_{2,3}}=\tau_p^2\mu\left(c_1\left(Q_2-Q_{f2}\mu\right)-Q_{f1}b_1\right)+\tau_p^2\left(b_2\left(Q_2-Q_{f2}\mu\right)+A_{11}Q_{f1}\right);$$

$$a'_{\psi_{2,4}}=-\tau_p^2\mu\left(c_1\left(Q_2-Q_{f2}\mu\right)+Q_{f1}b_1\right)+\tau_p^2\left(b_2\left(Q_2-Q_{f2}\mu\right)+A_{13}Q_{f1}\right);$$

Reference

1. Plunkett, A.B. and Plette, D.L, "Inverter-induction motor drive for transit cars," *IEEE Transactions on Industry Applications*, 1), pp. 26-37, (1977).
2. Lazi, J.M. Ibrahim, Z. Talib, M.H.N. and et al, "Dual motor drives for pmsm using average phase current technique," in *2010 IEEE International Conference on Power and Energy*, 2010: IEEE, pp. 786-790.
3. Lazi, J.M. Ibrahim, Z. and Sulaiman, M, "Mean and diffrential torque control using hysteresis current controller for dual pmsm drives," in *Journal of Theoretical and Applied information Technology*, 2011: Citeseer.
4. Xu, F. Shi, L. and Li, Y, "The weighted vector control of speed-irrelevant dual induction motors fed by the single inverter," *IEEE transactions on power electronics*, **28**(12), pp. 5665-5672, (2013).
5. Brando, G. Piegari, L. and Spina, I, "Simplified optimum control method for monoinverter dual parallel pmsm drive," *IEEE Transactions on Industrial Electronics*, **65**(5), pp. 3763-3771, (2017).
6. Lazi, J.M. Ibrahim, Z. Talib, M.H.N, and et al, "Non-independent speed control for dual-pmsm drives fed by a single three-leg vsi," **20**(pp. 1717-1724, (2020).

7. Ebadpour, M. Bannae Sharifian, M.B. and Babaei, E, "Modeling and control of dual parallel bldc motor drive system with single inverter," in *2017 International Electrical Engineering Congress (iEECON)*, 2017: IEEE, pp. 1-4.
8. Liu, T. and Fadel, M, "A controller proposed for mono-inverter multiple-pmsm system," in *Proc. 20th IFAC World Congr.*, 2017, vol. 50: Elsevier, pp. 14800-14805.
9. Liu, T. and Fadel, M, "An efficiency-optimal control method for mono-inverter dual-pmsm systems," *IEEE Transactions on Industry Applications*, **54**(2), pp. 1737-1745, (2017).
10. Ahmed, T. Kada, H. and Allali, A, "New dtc strategy of multi-machines single-inverter systems for electric vehicle traction applications," *International Journal of Power Electronics and Drive Systems*, **11**(2), p. 641, (2020).
11. Liu, T. Ma, X. Zhu, F. and et al, "Reduced-order feedback linearization for independent torque control of a dual parallel-pmsm system," *IEEE Access*, **9**(pp. 27405-27415, (2021).
12. Fadel, M. Nguyen, N.L. and Llor, A, "Direct torque control—a solution for mono inverter-dual parallel pmsm system," in *21st Mediterranean Conference on Control and Automation*, 2013: IEEE, pp. 1477-1483.
13. Jafari, M. Abbaszadeh, K. and Mohammadian, M, "A 12-sector space vector switching table for parallel-connecting to dual induction motors fed by matrix convertor based on direct torque control," *SN Applied Sciences*, **3**(11), pp. 1-14, (2021).
14. Rodriguez, J. Garcia, C. Mora, A. and et al, "Latest advances of model predictive control in electrical drives—part II: applications and benchmarking with classical control methods," *IEEE Transactions on Power Electronics*, **37**(5), pp. 5047-5061, (2021).
15. Nguyen, N.L. Fadel, M. and Llor, A, "Predictive torque control-a solution for mono inverter-dual parallel pmsm system," in *2011 IEEE International Symposium on Industrial Electronics*, 2011: IEEE, pp. 697-702.
16. Yu, Z. Du, Z. Wang, W. and et al, "Model predictive control method of dual pmsm fed by single inverter based on mtpa," in *2020 Chinese Automation Congress (CAC)*, 2020: IEEE, pp. 1477-1482.
17. Park, C. and Doki, S, "Active damping control method for different dual-parallel-spmsm systems with single inverter," *IEEJ Journal of Industry Applications*, p. 22006418, (2022).
18. Janouš, Š. Talla, J. Peroutka, Z. and et al, "Predictive control of parallel induction motors fed by single inverter with common current sensors," in *IECON 2018-44th Annual Conference of the IEEE Industrial Electronics Society*, 2018: IEEE, pp. 5843-5848.
19. Abbasi, M.A. and Husain, A.R.B, "Model predictive control of a dual induction motor drive fed by a single voltage source inverter," *Turkish Journal of Electrical Engineering & Computer Sciences*, **26**(3), pp. 1623-1637, (2018).
20. Adam, A.A. Purwadi, A. and Rohman, A.S, "Dual parallel induction motor fed by a single inverter based on two step predictive torque control,", *International Journal of Electrical Engineering and Informatic, (14), pp 698-724, (2022).*
21. Ratib, M.K. Alkhalaf, S. Senjyu, T. and et al, "Applications of hybrid model predictive control with computational burden reduction for electric drives fed by 3-phase inverter," *Ain Shams Engineering Journal*, p. 102028, (2022).
22. Nguyen, N.L. Fadel, M. and Llor, A, "A new approach to predictive torque control with dual parallel pmsm system," in *2013 IEEE International Conference on Industrial Technology (ICIT)*, 2013: IEEE, pp. 1806-1811.
23. Cimini, G. Bernardini, D. Bemporad, A. and et al, "Online model predictive torque control for permanent magnet synchronous motors," in *2015 IEEE International Conference on Industrial Technology (ICIT)*, 2015: IEEE, pp. 2308-2313.
24. Bouarfa, A. and Fadel, M, "Optimal predictive torque control of two pmsm supplied in parallel on a single inverter," *IFAC-PapersOnLine*, **48**(30), pp. 84-89, (2015).
25. Liu, T. and Fadel, M, "Performance comparison of control strategies for mono-inverter dual-pmsm system," in *2016 IEEE International Power Electronics and Motion Control Conference (PEMC)*, 2016: IEEE, pp. 637-642.
26. Cervone, A. Di Noia, L.P. Rizzo, R. Spina, I. and et al, "A constrained optimal model predictive control for mono inverter dual parallel pmsm drives," in *2018 7th International Conference on Renewable Energy Research and Applications (ICRERA)*, 2018: IEEE, pp. 1501-1507.
27. Koiwa, K. Kuribayashi, T. Zanma, T. and et al, "Optimal current control for pmsm considering inverter output voltage limit: model predictive control and pulse-width modulation," *IET Electric Power Applications*, **13**(12), pp. 2044-2051, (2019).
28. Li, T. Sun, X. Lei, G. and et al, "Finite-control-set model predictive control of permanent magnet synchronous motor drive systems—An overview," *IEEE/CAA Journal of Automatica Sinica*, (2022).
29. Fadaie Abras, M. Abbaszadeh, K. and Siadatan, A, "An energy-based predictive control with a fast real-time current-tuning for mono-inverter dual-parallel pmsm motors in power train application," *Journal of Control (English Edition)*, (2022).
30. Tauchnitz, N, "The pontryagin maximum principle for nonlinear optimal control problems with infinite horizon," *Journal of Optimization Theory and Applications*, **167**(1), pp. 27-48, (2015).
31. Held, M. Flärdh, O. and Mårtensson, J, "Optimal speed control of a heavy-duty vehicle in urban driving," *IEEE Transactions on Intelligent Transportation Systems*, **20**(4), pp. 1562-1573, (2018).
32. Xiao, Z. Wang, Q. Sun, P. and et al, "Real-time energy-efficient driver advisory system for high-speed trains," *IEEE Transactions on Transportation Electrification*, **7**(4), pp. 3163-3172, (2021).
33. Aalipour, A. Kebriaei, H. and Ramezani, M, "Analytical optimal solution of perimeter traffic flow control based on mfd dynamics: a pontryagin's maximum principle approach," *IEEE Transactions on Intelligent Transportation Systems*, **20**(9), pp. 3224-3234, (2018).
34. Fadaie, M. Abbaszadeh, K. and Siadatan, A, "Simplified and accurate predictive control method in mono-inverter dual-parallel permanent magnet synchronous motors," *International Journal of Industrial Electronics, Control and Optimization* (2022).
35. Cai, W. Wu, X. Zhou, M. and et al, "Review and development of electric motor systems and electric powertrains for new energy vehicles," *Automotive Innovation*, **4**(1), pp. 3-22, (2021).
36. Liu, T. and Fadel, M, "A controller proposed for mono-inverter multiple-pmsm system," *IFAC-Papers On Line*, **1**(50), pp. 14800-14805, (2017).

37. Bidart, D. Pietrzak-David, M. Maussion, P. and et al, "Mono inverter dual parallel pmsm-structure and control strategy," in *2008 34th Annual Conference of IEEE Industrial Electronics*, 2008: IEEE, pp. 268-273.

Figures and Tables Captions

Figure 1*. The drive structure of the multi-motor systems. (a) The control and feeding process of the motors separately. (b) The drive structure of MIDP Motors.*

Figure 2. *Block diagram of the proposed method. The EPC block in the outer loop is related to speed control and the PCC block in the inner loop is related to current control.*

Figure 3. *The dq rotating reference frame of the PMSM motors in the stationary system.*

Figure 4. *FCS-MPS structure in MIDP system*

Figure 5. *Speeds in start-up mode. (a-d) Speeds in the proposed method. (e-h) Speeds in FCS-MPC.*

Figure 6*. The commands used in the MIDP system and the speed response of the motors. (a) An overview on change procedures in speed command and load torque commands. (b) The speed performance of motors in proposed method. (c) The speed performance of motors in FCS-MPC method.*

Figure 7. *The torque waveforms of motors. (a) the torque performance of motors in proposed method. (b) the torque performance of motors in FCS-MPC method.*

Figure 8. *The phase-a current waveforms of motors. (a) I_a of both motors on the proposed method. (b) I_a of both motors on the FCS-MPC method.*

Figure 9. *Harmonic profile of phase-a currents. (a) and (b) are the current harmonics in the first and second motors on the proposed method, respectively. (c) and (d) are the current harmonics in the first and second motors on the FCS-MPC method, respectively.*

Figure 10. *Comparison of the cost function value on two methods.*

Figure 11. *Speed error of motors in two states. (a) and (b) are speed errors in EPC method in load and speed change, respectively. (c) and (d) are speed errors in conventional PI method in load and speed change, respectively.*

Figure 12. *Two strategies related to the MIDP system stability. (a) and (b) Reference speed in blue, the firs motor load torque in green, and the second motor load torque in red. (c) and (d) The electrical angle difference of the two rotors in degree.*

Figure 13. *The sensitivity of the proposed control method to change of the motor parameters. (a) Sensitivity controller to ψ_f . (b) Sensitivity controller to R_s . (c) Sensitivity controller to L_s .*

Table 1 PMSM motor parameters

Table 2 Three-phase inverter parameters

Table 3 Comparison of the proposed method to the FCS-MPC method.

Biography

Mehdi Fadaie received the M.S. degree in Electrical Engineering from the K. N Toosi University of Technology, Tehran, Iran, in 2010. He has been working toward the Ph.D. degree in electrical machines and drives in Department of Electrical Engineering of the Science and Research Branch, Azad University, Tehran, Iran. His thesis concerned model predictive control, permanent-magnet synchronous machines, voltage-source inverters, and mono-inverter dual-parallel motors. His main research activity concerns in research on advanced control techniques for motor drives and motion control and variable-speed applications. He is currently a faculty member of Islamic Azad University, Bojnourd.

Karim Abbaszadeh, received the B.S. degree in communication engineering from K. N. Toosi University of Technology, Tehran, Iran, in 1991, and the M.S. and Ph.D. degrees in electrical engineering from Amir Kabir University of Technology, Tehran, Iran, in 1997 and 2000, respectively, From 2001 to 2003. He was a Research Assistant with the Department of Electrical Engineering, Texas A&M University, and College Station, TX, USA. He became an Assistant Professor in 2002, an Associate Professor in 2007, and a Full Professor of power electronics and electrical machine and drives in 2012; He is

currently a full Professor with the Department of Electrical Engineering, K. N. Toosi University of Technology. His current research interests include power electronics and its applications such as in wind turbines, PV systems, electric machinery, and variable-speed drives. He has published more than 100 journal papers in the fields of power electronics and its applications. He is the author of two books in power electronics and its applications. He is actively involved in presenting short courses and consulting in his area of expertise to various industries.

Alireza Siadatan (S'07, M'13, SM'18) received the B.Sc., Ph.D. and Postdoc degrees in electrical engineering from Shahid Beheshti University G.C., Tehran, IRAN, in 2002, 2013 and 2014, respectively, and the M.Sc. degree in electrical engineering from Azad University, south Tehran branch. He was a Visiting Student in Wisconsin University at Madison, 2012, USA. He has published around 170 Journal and conference papers and 15 patents. He joined the Azad University, West Tehran Branch, Iran, in 2008. Currently, He is a Visiting Professor at University of Toronto, CANADA. His current research interests include electric machines design and drives, BCI, renewable energy, special machines such as SRM, SynRM and power electronics.

Figures:

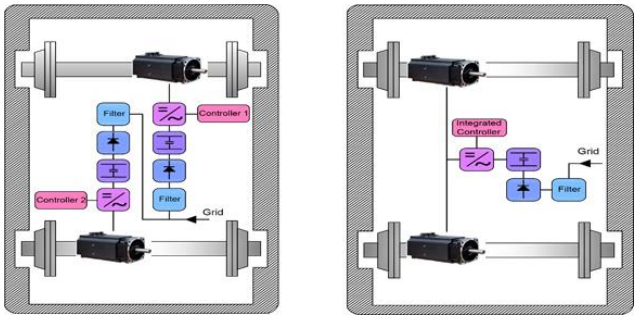

(a) (b)

Figure 1. *The drive structure of the multi-motor systems. (a) The control and feeding process of the motors separately. (b) The drive structure of MIDP Motors.*

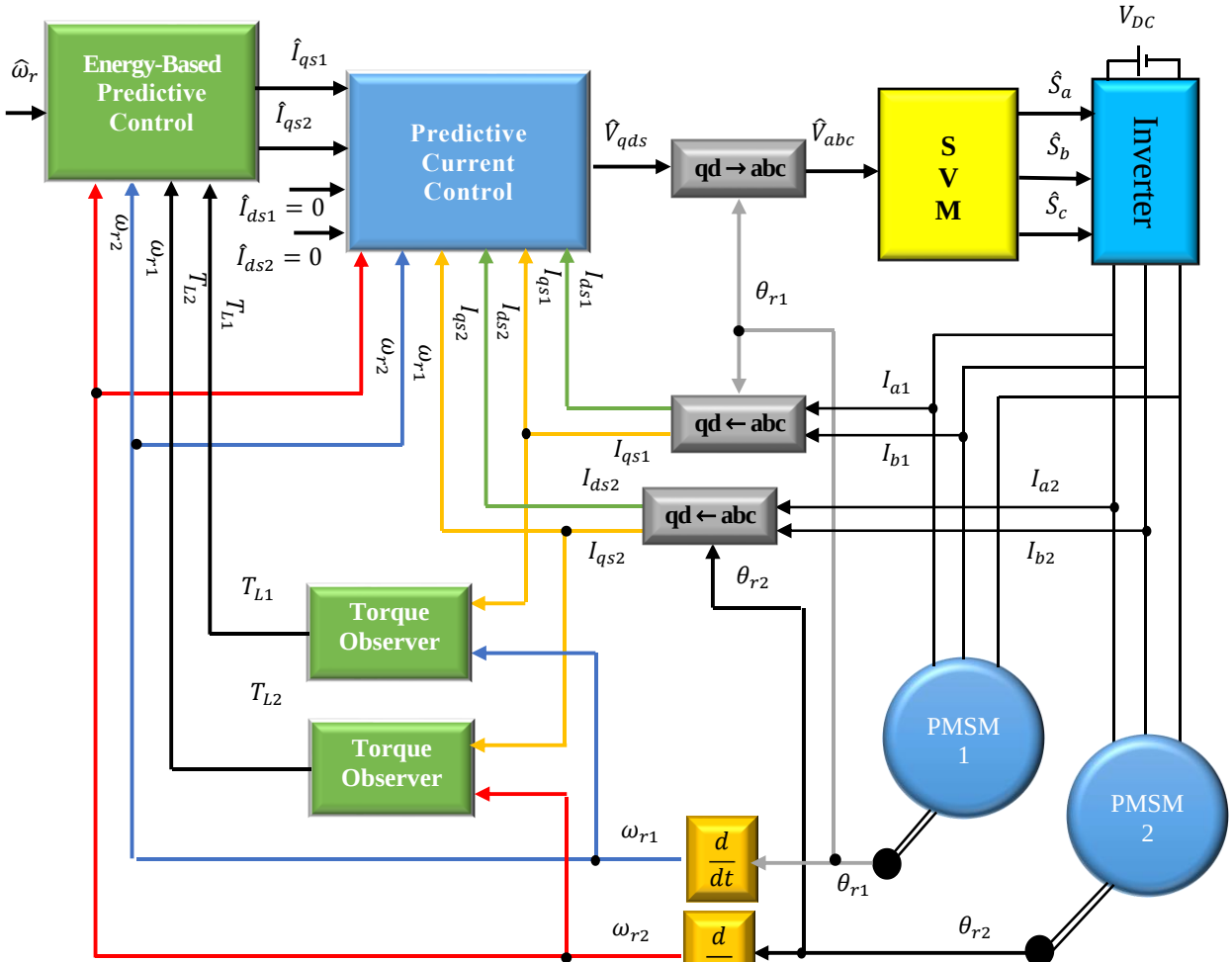

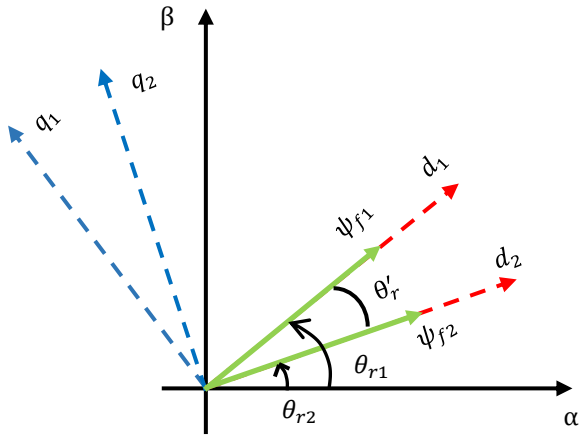

Figure 3. *The qd rotating reference frame of the PMSM motors in the stationary system.*

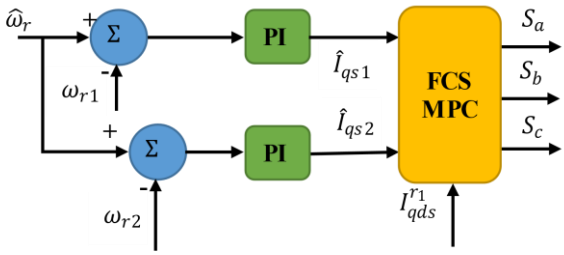

Figure 4. *FCS-MPS structure in MIDP system*

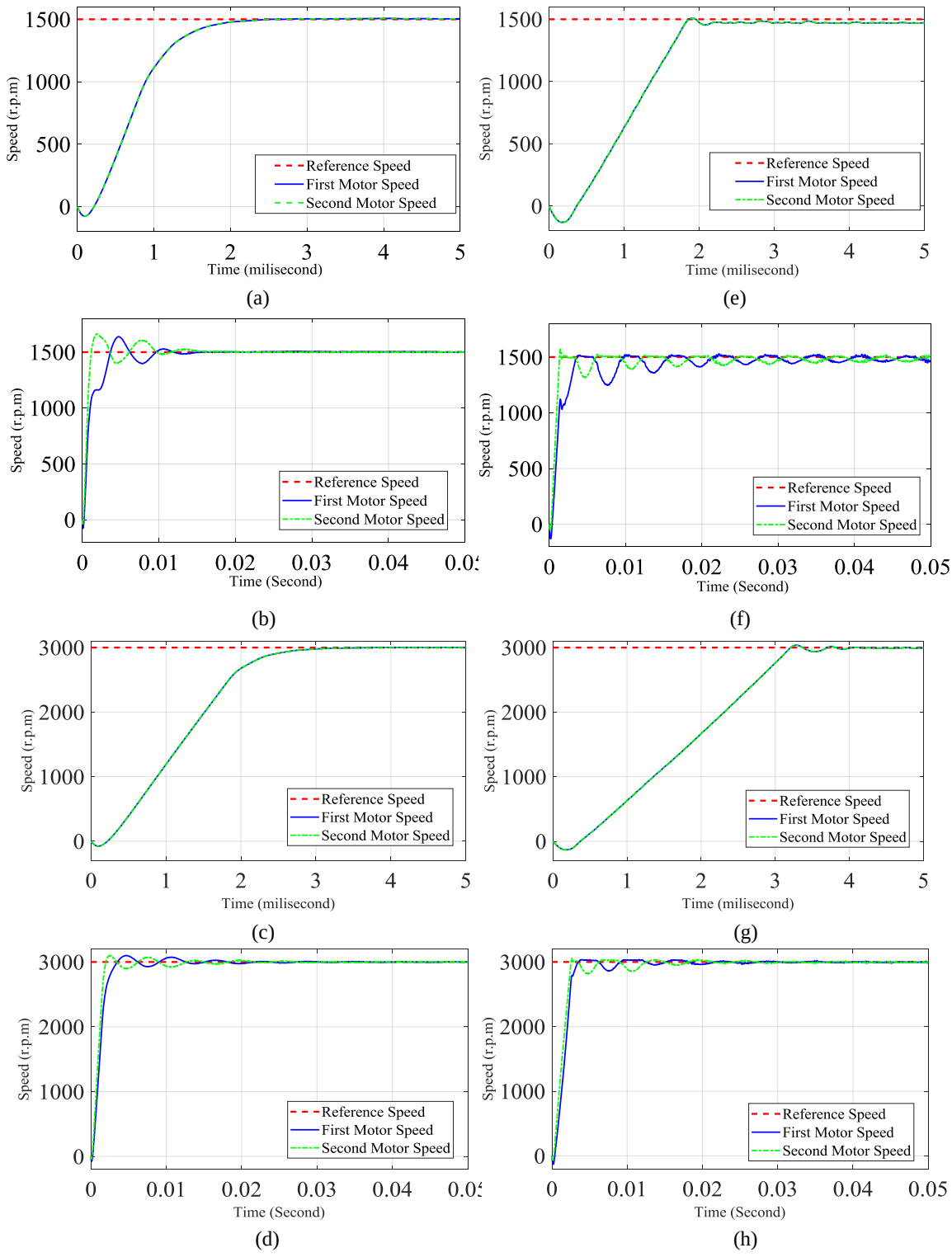

Figure 5. *Speeds in start-up mode. (a-d) Speeds in the proposed method. (e-h) Speeds in FCS-MPC.*

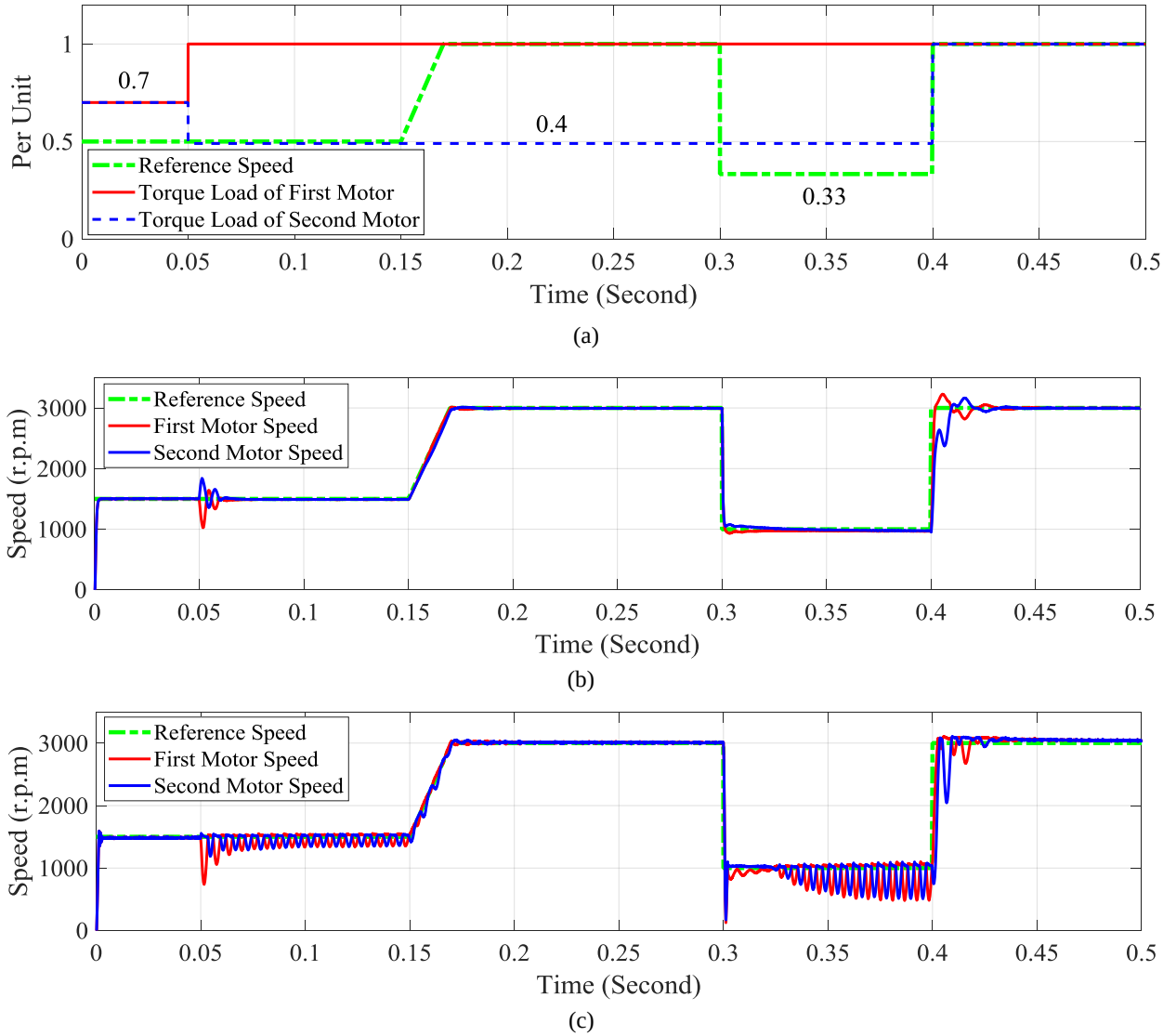

Figure 6. *The commands used in the MIDP system and the speed response of the motors. (a) An overview on change procedures in speed command and load torque commands. (b) The speed performance of motors in proposed method. (c) The speed performance of motors in FCS-MPC method.*

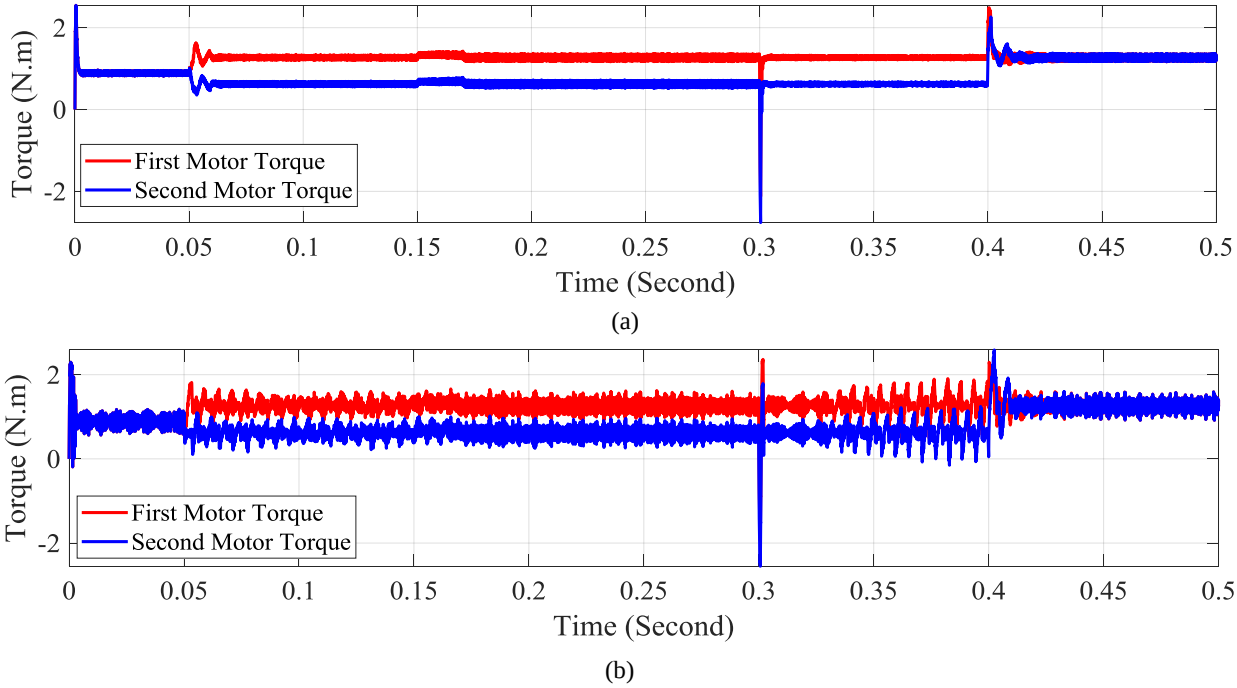

Figure 7.*The torque waveforms of motors. (a) the torque performance of motors in proposed method. (b) the torque performance of motors in FCS-MPC method.*

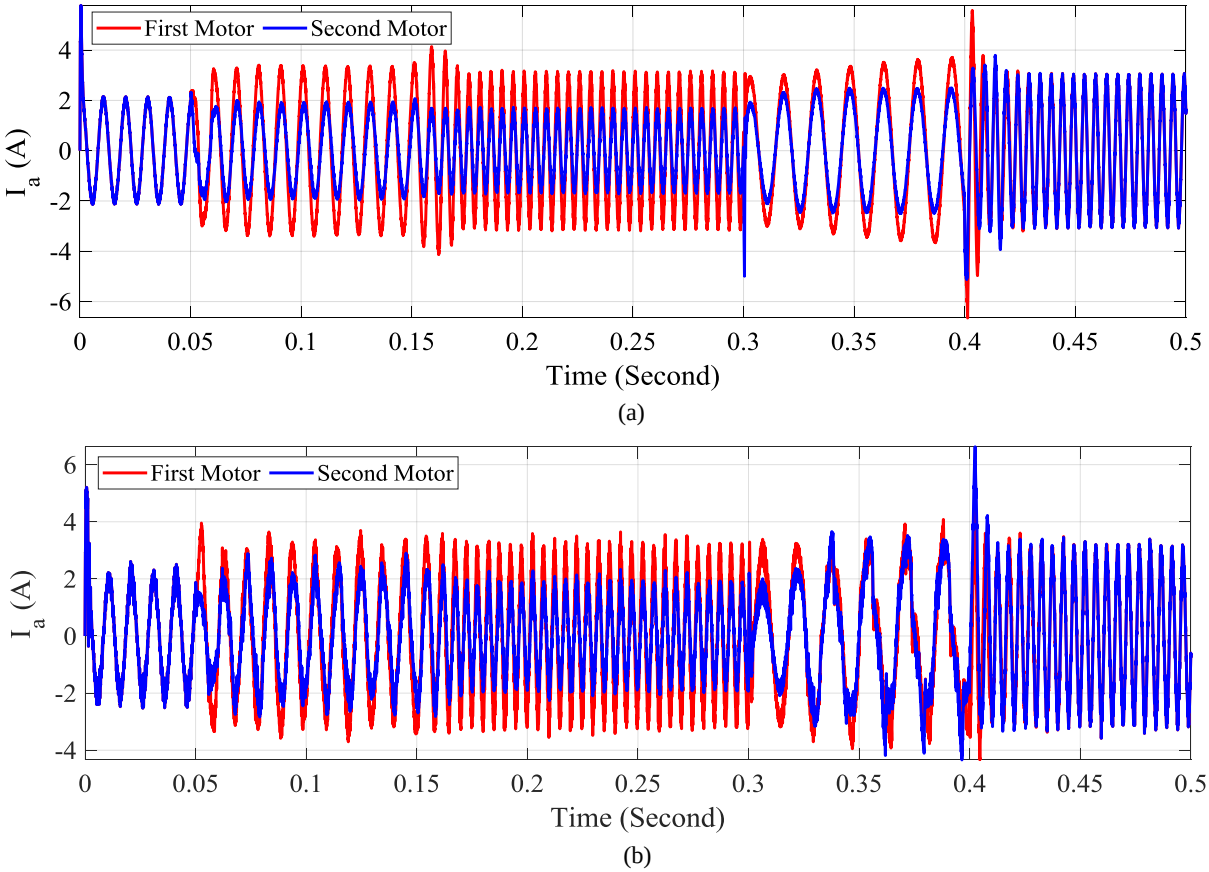

Figure 8. *The phase-a current waveforms of motors. (a)* I_a *of both motors on the proposed method. (b)* I_a *of both motors on the FCS-MPC method.*

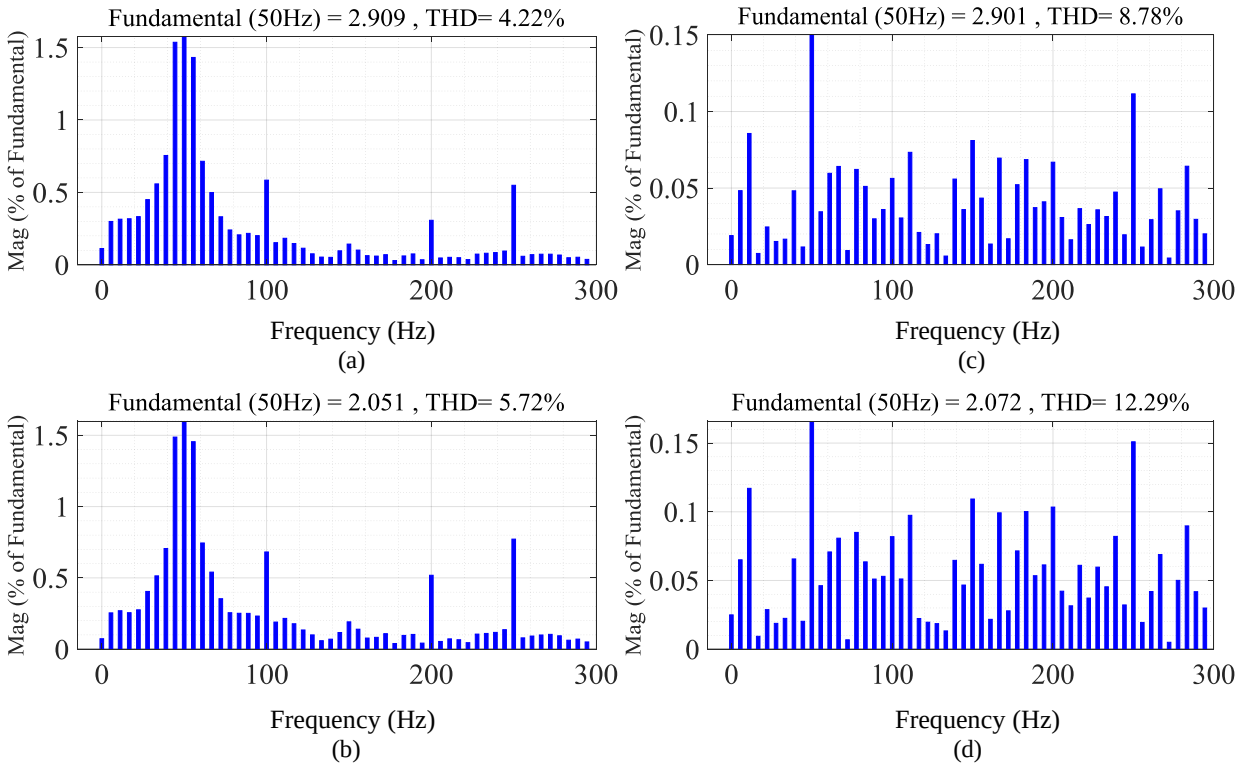

Figure 9. *Harmonic profile of phase-a currents. (a) and (b) are the current harmonics in the first and second motors on the proposed method, respectively. (c) and (d) are the current harmonics in the first and second motors on the FCS-MPC method, respectively.*

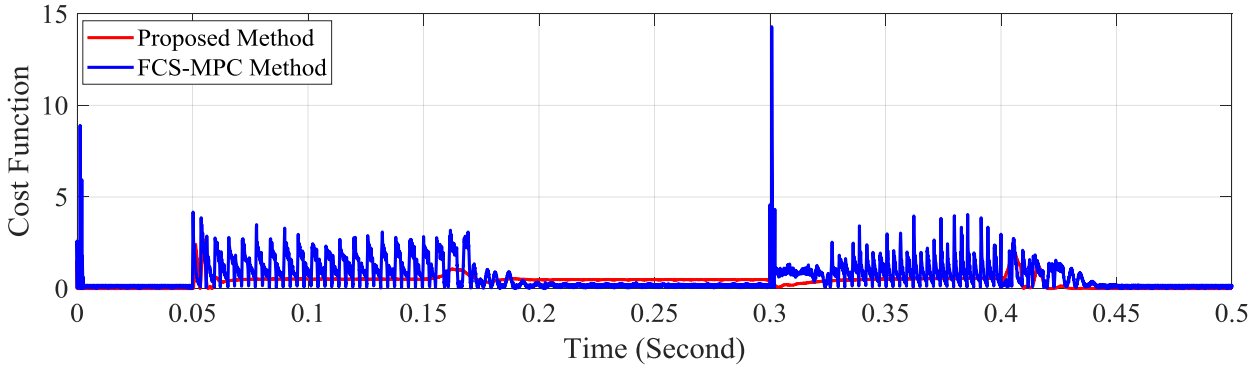

Figure 10. *Comparison of the cost function value on two methods.*

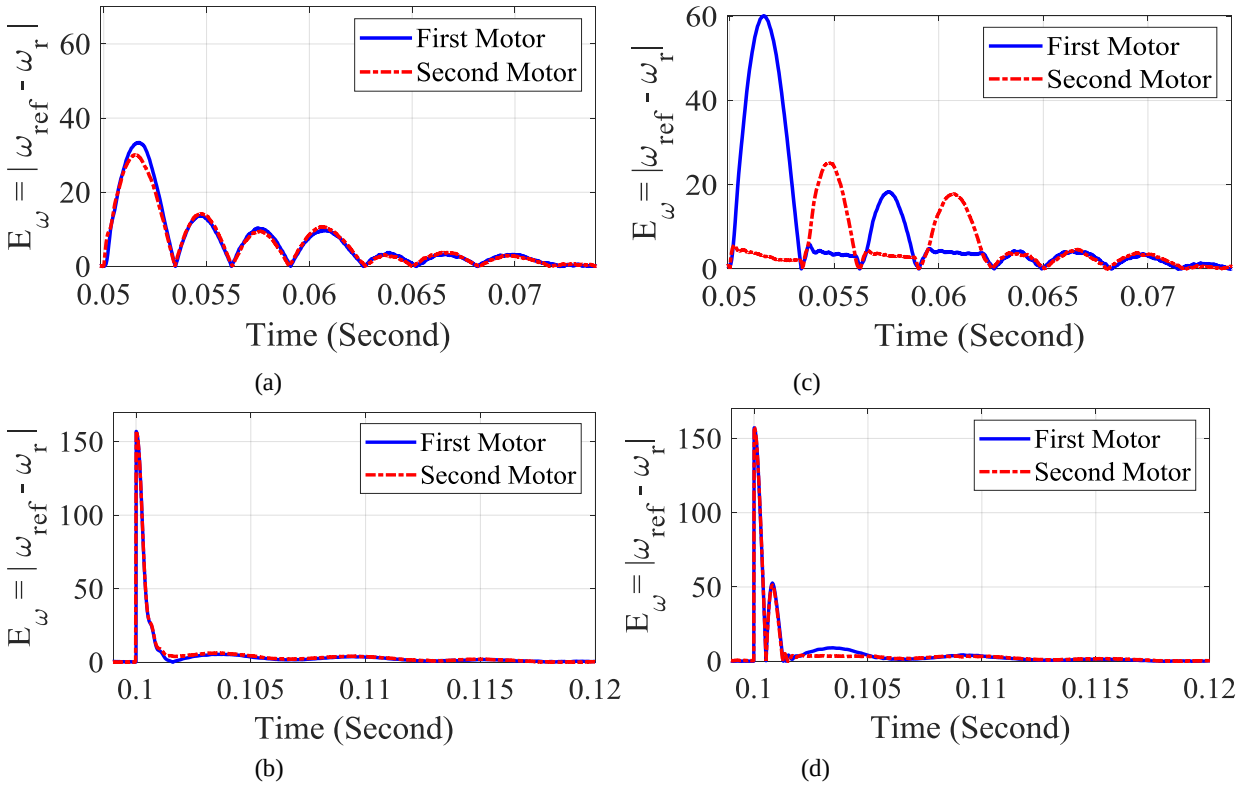

Figure 11*.Speed error of motors in two states. (a) and (b) are speed errors in EPC method in load and speed change, respectively. (c) and (d) are speed errors in conventional PI method in load and speed change, respectively.*

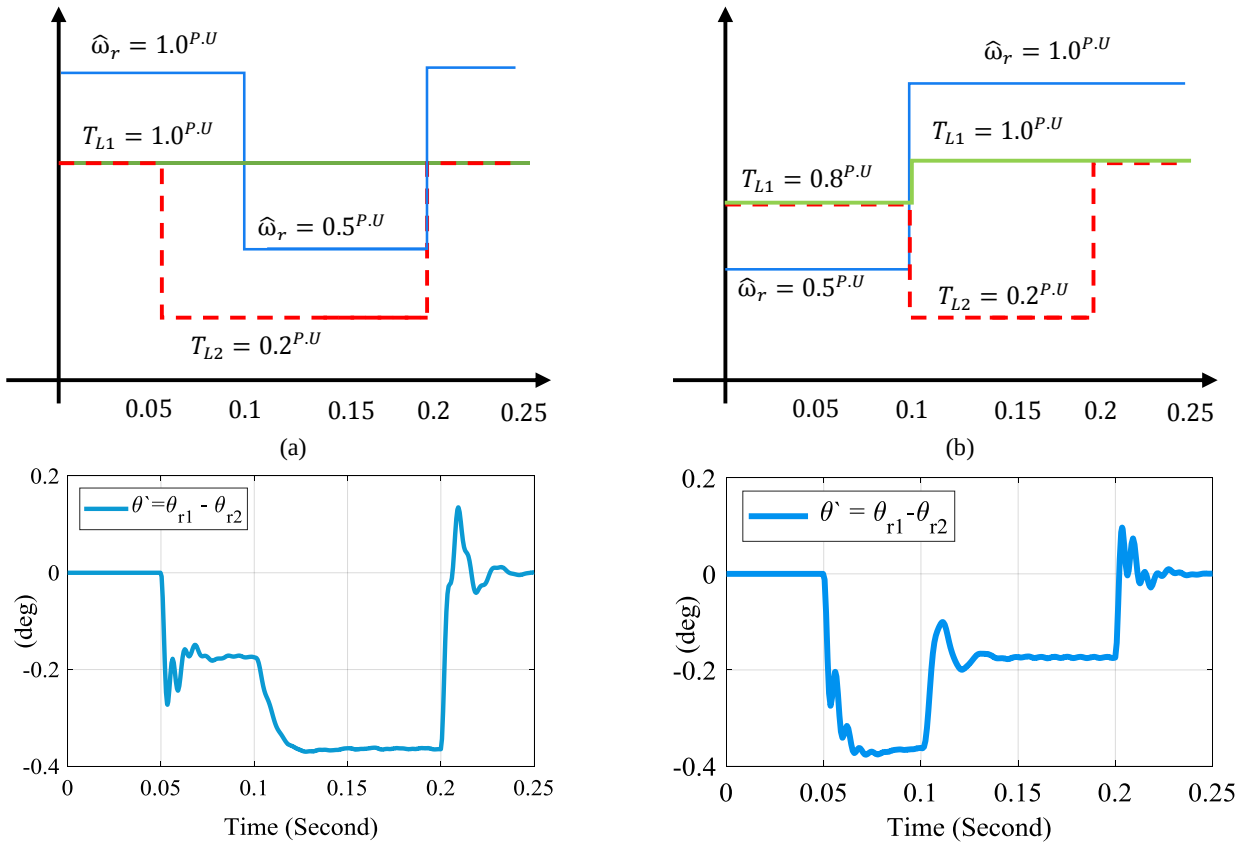

Figure 12. *Two strategies related to the MIDP system stability. (a) and (b) Reference speed in blue, the firs motor load torque in green, and the second motor load torque in red. (c) and (d) The electrical angle difference of the two rotors in degree.*

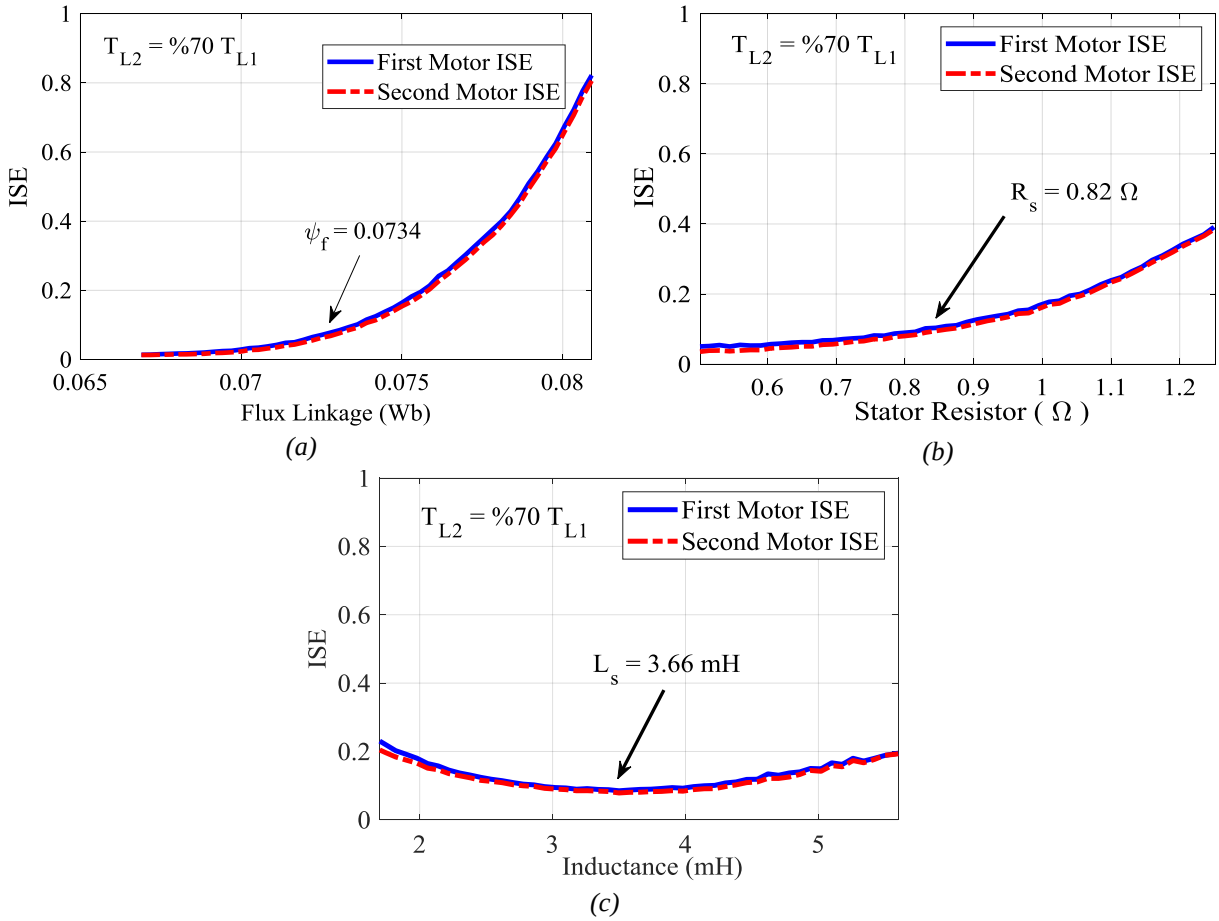

Figure 13. *The sensitivity of the proposed control method to change of the motor parameters. (a) Sensitivity controller to* ψ_f *. (b) Sensitivity controller to* R_s *.(c) Sensitivity controller to* L_s *.*

Tables:

Table 1 PMSM motor parameters

Motor Parameter		**Parameter Value**
Nominal Power	P_{rate}	400^{watt}
Nominal Current	I_{rate}	2.89^{A}
Total Number of Poles	p	8
Stator Resistance	r_s	0.82^{Ω}
Stator Inductance	L	3.66^{mH}
Permanent Magnet Flux	ψ_f	0.0734^{wb}
Nominal Speed	N_{syn}	$3000^{r.p.m}$
Nominal Torque	T_{rate}	$1.27^{N.m}$
Maximum Torque	T_{max}	$3.82^{N.m}$
Moment of Inertia	J	$0.0321\times10^{-4\ Kg.m^2}$
Friction Coefficient	B_m	$0.6\times10^{-6\ N.m.Sec}$

Table 3 Comparison of the proposed method to the FCS-MPC method.

	Proposed MPC		**FCS-MPC**	
	M_1	M_2	M_1	M_2
Total Harmonic Distribution (THD)	4.22%	5.72%	8.78%	12.29%
Max Speed Deviation in Braking Process Up to 66.7% of the Nominal Speed	Less Than $80^{r.p.m}$	Less Than $80^{r.p.m}$	More Than $800^{r.p.m}$	More Than $800^{r.p.m}$
Simultaneous control capability of Parallel Motors	Able		Unable	
Switching Frequency	Constant		Variable	
Voltage Modulator	Necessary		Not Necessary	
Dependence of Settling Time on Commands at Start-Up	Almost Independent		Dependence	
The Number of Multiplication and Addition Operators in any Control Cycle	Multi 104	Add 132	Multi 342	Add 168

Table 2 Three-phase inverter parameters

Inverter Parameter		**Parameter Value**
DC Power Supply	V_{DC}	173^{V}
Switching Frequency	f_{SW}	8^{KHz}
On-Mode Switch Resistance	$R_{DS(on)}$	0.019^{Ω}